A&A 374, 1121–1126 (2001)
DOI: 10.1051/0004-6361:20010802

Astronomy & Astrophysics

A possible broadening mechanism of He I 10 830 Å profiles observed in a limb flare

H. Li and J. You

Purple Mountain Observatory, National Astronomical Observatories, Nanjing 210008, PR China

Received 8 September 2000 / Accepted 17 May 2001

Abstract. The He I 10 830 Å spectra observed in the impulsive phase of the 2N/X20 solar limb flare of 16 August 1989 show unusually broad profiles, and most of the profiles are blue-shifted and/or blue asymmetric with full-width-at-half-maximum (*FWHM*) greater than 10 Å. Contrary to prominences, weak post-flare loops and surges, the observed profiles of the flare cannot be simulated by Doppler broadening with a uniform flaring atmosphere model. Calculations show that only when the electron density is greater than 10^{16} cm^{-3} can Stark broadening produce an obvious influence on the He I 10 830 Å profile. This indicates that it is not plausible that Stark broadening leads to the observed profiles even though they can be fitted by Stark broadening. Alternatively, an expanding flaring atmosphere can perfectly simulate all the observed He I 10 830 Å profiles. The expanding velocities are generally several tens of km s^{-1} and that corresponding to the widest profile is greater than 120 km s^{-1}. Expanding velocity and other parameters vary with time and the observed area. This expanding flaring atmosphere model is a perspective candidate for line broadening. It is an indication of the lateral expansion resulting from rapid chromospheric heating in addition to the upward evaporation and downward condensation.

Key words. Sun: flares – Sun: infrared – line: profiles

1. Introduction

The dynamical process of a chromospheric flare has been studied numerically since the early 1980's (Fisher et al. 1985). The predicted upward chromospheric evaporation and downward chromospheric condensation, resulting from sudden heating of the chromosphere by non-thermal electrons or thermal conduction, have been more or less confirmed by observations of the blue-shift of EUV lines and the red asymmetry of the Hα line, respectively (Fisher et al. 1985). Large blue shifts in limb flares were previously observed (Gaizauskas 1986; Graeter & Kucera 1992), implying horizontal expansion or motion in limb flare at heights <3000 km. However, there is no theoretical study of the lateral effect of the chromospheric heating so far, for all the models are one-dimensional. The best way to investigate this effect is to observe and study solar limb flares.

We obtained a series of He I 10 830 Å profiles of two limb flares occurring in AR 5629 on 16 and 17 August 1989 (2N/X20 and SF/X2.9 respectively). We study the 2N/X20 flare of 16 August in this paper. The observed spectra are quite suitable for a study of the lateral effect: first, the flare took place near the limb (S16W88) and we got complete data of the 16 August flare; second, the He I 10 830 Å triplet, which comprises I_{12} (10 830.341 Å + 10 830.250 Å) and I_3 (10 829.081 Å), has the unique advantage of diagnosing the physical parameters of the solar flare due to its high excitation potential. Meanwhile, its much higher excitation potential than hydrogen and Ca II makes it a special diagnostic tool for studying the hotter and denser flare atmosphere (Lites et al. 1986). Moreover, the absorption of the He I 10 830 Å line is rather less than Hα on the solar disk, therefore, it can observe a lower part of solar flare than the Hα when the flare occurs near the solar limb.

Contrary to the appearance in disk flares, where He I 10 830 Å spectra show red shift and/or red asymmetry (You et al. 1993; Ichimoto et al. 1993) due to a downward moving chromosphere condensation (Fisher et al. 1985), all the observed He I 10 830 Å profiles of the 16 August 1989 flare show blue shift and/or blue asymmetry (You et al. 1998) and have more or less non-thermal broadening wings. Most of the profiles have *FWHM* greater than 10 Å and cannot be simulated by Doppler broadening with a uniform flaring atmosphere model. One of the studies (You & Oertel 1992) fitted the widest He I 10 830 Å profile ("full width" >20 Å) observed in

Send offprint requests to: H. Li,
e-mail: lihui@mail.pmo.ac.cn

the impulsive phase using Stark broadening and got an electron density as high as 4×10^{17} cm^{-3}. We simulate other observed He I 10 830 Å profiles by Stark broadening in this paper and get similar results (Sect. 3.2). Then we try to invoke a non-uniform flaring atmosphere model to fit the observed profiles (Sect. 3.3).

In the sections following, we introduce the observations and data reduction (Sect. 2), and simulate the observed He I 10 830 Å profiles in three ways (Sect. 3). The discussions and conclusions are presented in Sect. 4.

2. Observation and data reduction

The observation was made with the one-dimensional Reticon system (Wang et al. 1987; Li et al. 1999) mounted on the multichannel spectrograph at the Purple Mountain Observatory. The spatial resolution is $0.5'' \times 3''$, and the line dispersion is 1.943 Å mm^{-1}, corresponding to a sampling interval of 1.3 km s^{-1} per pixel. The integration time was 10 s. We scanned the flaring area once every 30−90 s. The spectra of disk center and nearby background provided an intensity calibration. The solar image around the slit was monitored and photographed simultaneously with He I 10 830 Å in Hα (0.5 Å passband) with a slit-jaw system.

The raw data were processed in the following way (Wang et al. 1989): (1) dark-current and flat-field correction; (2) subtraction of the scattered light in the spectrograph; (3) image restoration for removing the instrumental profile of the system, including cross-talk of the Reticon array.

The 2N/X20 flare discussed in this paper took place in NOAA 5629 at 00:59 UT on 16 August 1989, peaked at 01:19 UT and ended at 02:17 UT based on our Hα observation. Our slit-jaw Hα photography began at 00:15 UT, 44 min before the flare onset. The He I 10 830 Å observation started at 00:47:13 UT, and continued until 02:36:50 UT. Since the shape and height of the limb flare changed rapidly during the impulsive phase, we usually selected the brightest parts of the flare in Hα as the target for He I 10 830 Å observations. Whenever a limited area of the flare was relatively stable for a short time, we kept the slit on that target for a series of spectrograms.

Since the flare profiles are unusually broadened, the two components of HeI line, I_{12} and I_3, affect each other. So instead of the traditional bisector method, we used another method to determine the velocity – comparing the theoretical profiles with the observed ones.

3. Simulations of the observed profiles

The shape of a spectral line is often used to assess the temperature, microturbulence and the density of the radiating plasma. When assuming a uniform flaring atmosphere with a constant source function the intensity of the He I 10 830 Å line observed in a limb flare is (You et al. 1989)

$$I_\lambda = S_\lambda \cdot (1 - \mathrm{e}^{-\tau_\lambda}) \tag{1}$$

and the optical thickness

$$\tau_\lambda = \tau_{03} \left[5\mathrm{e}^{-\frac{(\Delta\lambda-\Delta\lambda_0)^2}{\Delta\lambda_\mathrm{D}^2}} + 3\mathrm{e}^{-\frac{(\Delta\lambda+0.091-\Delta\lambda_0)^2}{\Delta\lambda_\mathrm{D}^2}} + \mathrm{e}^{-\frac{(\Delta\lambda+1.26-\Delta\lambda_0)^2}{\Delta\lambda_\mathrm{D}^2}} \right] \tag{2}$$

in the Doppler broadening only case, where, $\Delta\lambda = \lambda - \lambda_0$ ($\lambda_0 \equiv \lambda_{ij}$), $\Delta\lambda_0 = \frac{\upsilon}{c}\lambda_0$, and τ_{03} is the line-center optical thickness of I_3 component of the triplet. And

$$\tau_\lambda = \tau_{03} \cdot \left\{ 5H\left[a_1, u\left(\frac{\Delta\lambda - \Delta\lambda_0}{\Delta\lambda_\mathrm{D}}\right)\right] + 3H\left[a_2, u\left(\frac{\Delta\lambda + 0.091 - \Delta\lambda_0}{\Delta\lambda_\mathrm{D}}\right)\right] + H\left[a_3, u\left(\frac{\Delta\lambda + 1.26 - \Delta\lambda_0}{\Delta\lambda_\mathrm{D}}\right)\right] \right\} \tag{3}$$

in the case of Doppler broadening coupled with the damping broadening. Here

$$H(a,u) = \frac{a}{\pi}\int_{-\infty}^{+\infty} \frac{\mathrm{e}^{-y^2}}{a^2 + (u-y)^2}\mathrm{d}y \tag{4}$$

is the Voigt function and $y = \frac{\Delta\nu}{\Delta\nu_\mathrm{D}}$, $u = \frac{\nu-\nu_{ij}}{\Delta\nu_\mathrm{D}}$, $a = \frac{\delta_{ij}}{\Delta\nu_\mathrm{D}}$.

3.1. Uniform flaring atmosphere model

We chose a uniform flaring atmosphere model and try to model the observed profiles by Doppler broadening in two ways, but neither reproduce the observed profile very well (Fig. 1a). First, we simulated the observed profile with $\Delta\lambda_\mathrm{D} = 0.56$ Å, and the computed profile shows a swell on the blue wing at wavelength of I_3. But the calculated I_3 is weaker than the observed one and has much narrower wings (Fig. 1a, dashed line). We then used a rather large $\Delta\lambda_\mathrm{D}$ (1.1–1.2 Å) to fit the profile. The result matches the wings of observed profile on the whole, but not the line-center (Fig. 1a, solid line). Since the absorption in I_3 is much weaker than I_{12}, it is improbable that the swelling on the blue wing is caused by a central reversal.

On the other hand, the He I 10 830 Å profiles of a weak rising post-flare loop and a flare-associated surge can be perfectly simulated by Doppler broadening with a uniform flaring atmosphere model. Figure 1b shows the observed He I 10 830 Å profile (dotted line) of a flare-associated surge and the computed profile (solid line) using Doppler broadening.

Based on the above calculation, we conclude that the assumptions – a uniform model atmosphere and a pure Doppler broadening mechanism – are not satisfied for this limb flare.

3.2. Effect of Stark broadening

For the He I 10 830 Å line, the Stark effect due to electrons is considerably larger than that due to other particles; linear Stark broadening of electrons is much smaller than

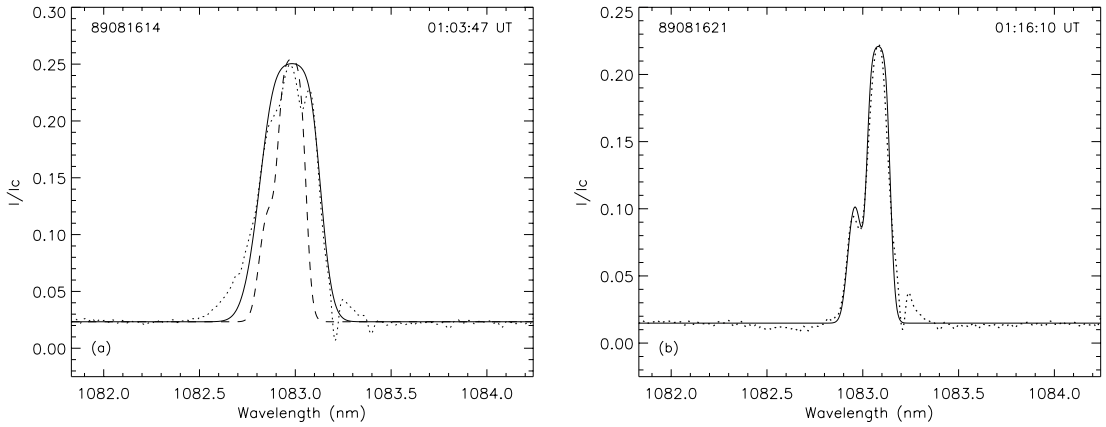

Fig. 1. a) Observed He I 10 830 Å profile (dotted line) at 01:03:47 UT on 16 August 1989 and the fitted profile by Doppler broadening with a uniform flaring atmosphere model with $\tau_{03} = 0.5$, $S = 490$, $\Delta\lambda_D = 0.56$ Å, $v_d = 14$ km s^{-1} (dashed line), and that with $\tau_{03} = 0.5$, $S = 480$, $\Delta\lambda_D = 1.1$ Å, $v_d = 12$ km s^{-1} (solid line). **b)** Observed profile of a flare-associated surge (dotted line) and the fitted one (solid line) with $\tau_{03} = 0.46$, $S = 440$, $\Delta\lambda_D = 0.48$ Å and $v_d = -14$ km s^{-1} by Doppler broadening. Source functions in this paper are given in units of $I_c/2080$, where $I_c = 1.027 \times 10^{10}$ erg ster^{-1} cm^{-2} μm^{-1} s^{-1} is the disk-center intensity of continuum around 10 830 Å.

quadratic Stark broadening. Therefore, in practical computations, it is acceptable to only take into account the quadratic Stark broadening. Then δ_{ij} can be written as

$$\delta_{ij} = \frac{1}{4\pi}(\gamma_i + \gamma_j + \gamma_3 + \gamma_4 + \gamma_6) \tag{5}$$

γ_i and γ_j is the spontaneous transition coefficient of the involved lower and upper level. In our case, $\gamma_i = 0$ as the lower level of the transition is metastable. γ_3, γ_4, γ_6 is the collisional damping coefficient of helium with ambient helium, electrons and other neutral atoms or molecules.

$$\gamma_3 = 4\pi^3 C_3 N, \quad \gamma_4 = 38.8 C_4^{2/3} \bar{v}^{1/3} N,$$
$$\gamma_6 = 17.0 C_6^{2/5} \bar{v}^{3/5} N, \quad \bar{v} = \sqrt{\frac{8RT}{\pi}(\frac{1}{\mu_1} + \frac{1}{\mu_2})} \tag{6}$$

where N is the number density of the disturbing particle. C_n ($n = 3,\ 4,\ 6$) is a constant related to n that can be calculated by a quantum mechanical method. Calculations show that γ_3 and γ_6 are much smaller than γ_4 for the HeI infrared triplet.

To compare the effects of Doppler and Stark broadening on the He I 10 830 Å profile, we computed the He I 10 830 Å profile using Doppler broadening and Stark broadening separately with a set of parameters and different electron densities. The results are shown in Fig. 2. We notice from Fig. 2 that Stark broadening profiles with $N_e = 10^{15}$ cm^{-3} and 5×10^{15} cm^{-3} are almost the same as the Doppler broadening profile (solid line). The profile with $N_e = 10^{16}$ cm^{-3} has a slightly lower peak intensity and little difference in the wings of the profile. The difference becomes more and more significant as N_e increases. Namely, for the He I 10 830 Å line, the Stark effect will be significant only when the electron density is greater than 10^{16} cm^{-3} .

We try to fit the observed profiles by Stark broadening because most of them have a Doppler core and Lorentz wings. Figure 3a shows one of the observed profiles at

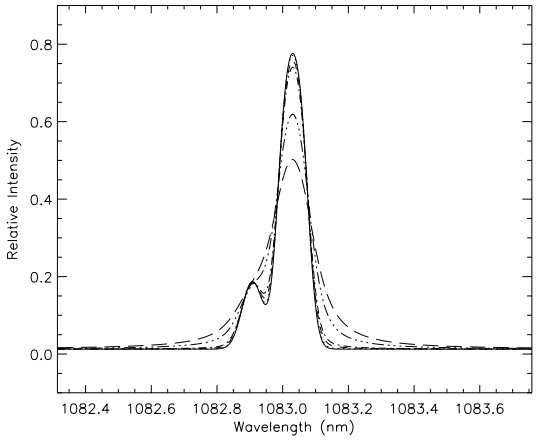

Fig. 2. Comparison of He I 10 830 Å profiles produced by Doppler broadening mechanism with $\tau_{03} = 0.2$, $S_\lambda = 2000$, $T_e = 10^4$ K and $\xi_t = 15$ km s^{-1} (solid) and Stark broadening mechanism with above parameters and $N_e = 10^{15}$ (dotted), 5×10^{15} (dashed), 10^{16} (dash dot), 5×10^{16} (dash dot dot dot) and 10^{17} cm^{-3} (long dash).

01:10:54 UT (dotted line) and the modeled one (dashed line) by Stark broadening. The required electron density ($N_e = 4 \times 10^{17}$ cm^{-3}) is about 4–5 orders higher than the generally accepted one in large flares. The temperature of the chromospheric flare is about 10 000 K, at which most of the helium is in the neutral state. Such a high electron density indicates that the optical thickness of the He I 10 830 Å line is rather large, and the profile should show a flat top due to strong central saturation. However, we did not detect any such He I 10 830 Å profile during the whole flaring process. Therefore, it is improbable that Stark broadening leads to the observed unusually broad profile.

3.3. Expanding flaring atmosphere model

Actually, the atmosphere along the horizontal direction relative to the solar disk should not be uniform because

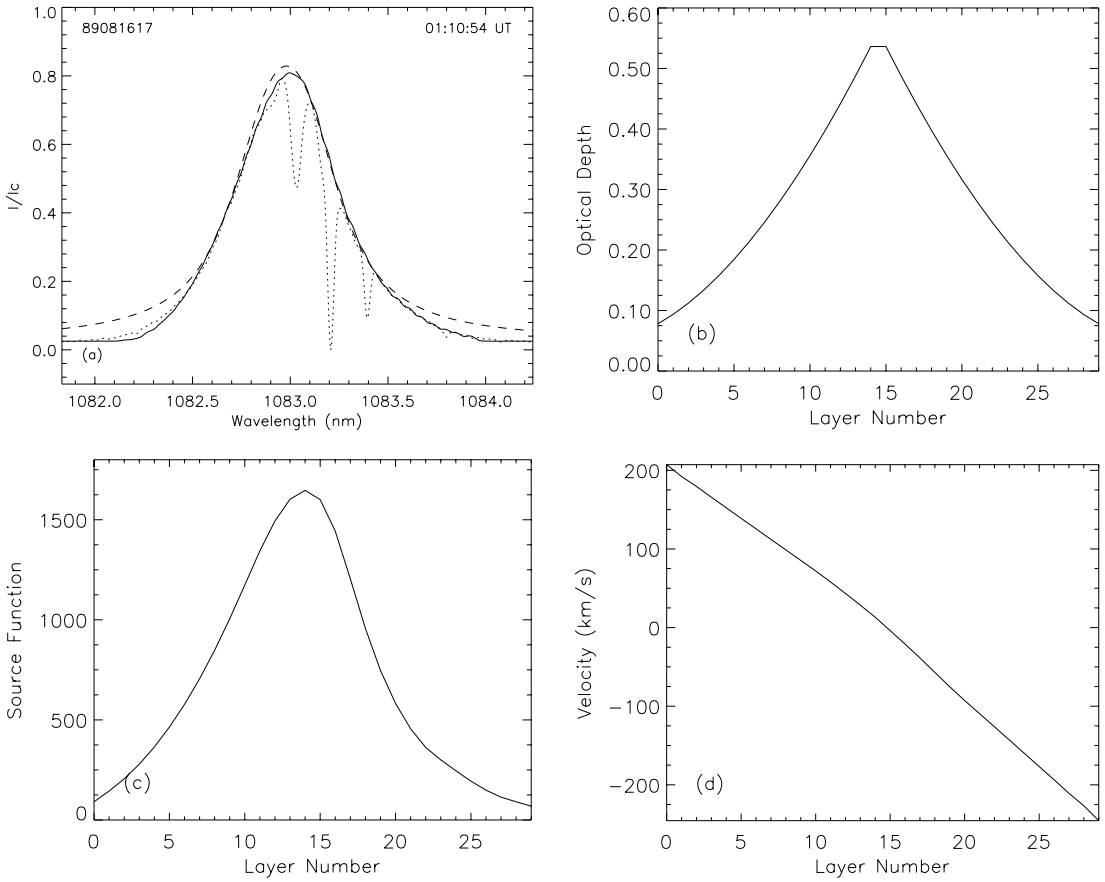

Fig. 3. a) He I 10 830 Å profile taken at 01:10:54 UT on 16 August 1989 (dotted line), the computed profile by expanding flare model (solid line) and that by Stark broadening with $\tau_{03} = 0.5$, $S = 2200$, $\Delta\lambda_D = 1.1$ Å, $\upsilon_d = 12$ km s^{-1} and $N_e = 4\times10^{17}$ cm^{-3} (dashed line). The observation time is indicated at the upper-right corner. **b)-d)** Distributions of the corresponding optical depth τ_{03}, source function S (solid line), and Doppler velocity υ_d respectively.

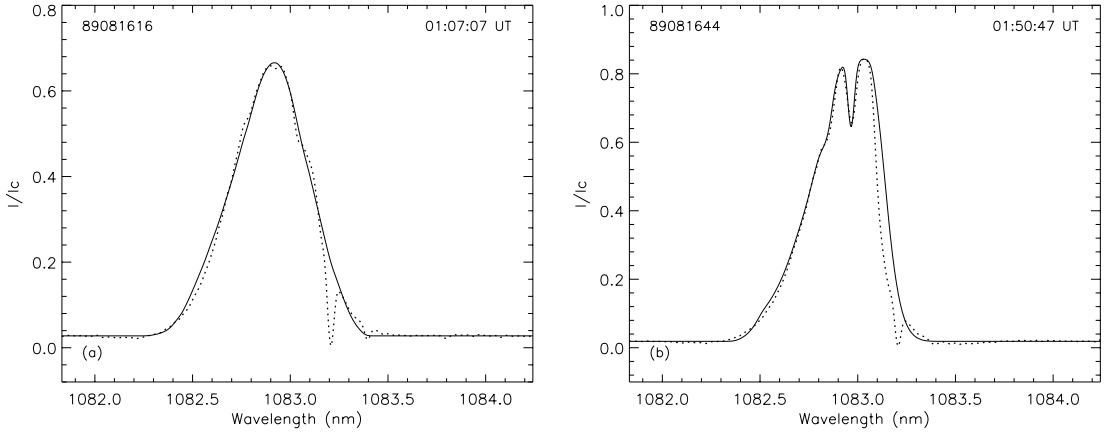

Fig. 4. a) He I 10 830 Å profile taken at 01:07:07 UT on 16 August 1989 (dotted line) and the computed profile (solid line), I_c is the disk-center intensity of the continuum around 10 830 Å. The observation time is indicated at the upper-right corner. **b)** same as **a)** but for the profile taken at 01:50:47 UT.

of the downward motion of chromospheric condensation resulting from the large amount of energy transported to the chromosphere. We propose an alternative: an expanding flaring atmosphere model to interpret the observed He I 10 830 Å profiles. In this model, we assume certain distributions of physical parameters along the line-of-sight, which include optical depth of the I_3 component τ_{03}, source function S, electron temperature T_e, non-thermal velocity ξ_t and Doppler velocity υ_d that consists of the expanding velocity υ_{exp} and macro-shift velocity υ_{mac} ($\upsilon_d = \upsilon_{exp} + \upsilon_{mac}$). Actually, S, τ_{03} and T_e are not independent. In our computation, for the first order

approximation, the electron temperature T_e was taken to be 10^4 K. This will not affect the result much because the Doppler width is not sensitive to the temperature and the observed profiles are very wide. In this paper, we will mainly investigate the effect of expanding velocity, source function and optical depth.

In practise, to address this problem, we divided the flaring atmosphere into a certain number of layers, say n for example ($n \geq 2$), and each layer is treated as uniform where Eq. (1) is applicable. Then the intensity of the line is

$$I_\lambda = (1-e^{-\tau_{\lambda,1}}) \cdot S_{\lambda,1} + \sum_{i=2}^{n} (1-e^{-\tau_{\lambda,i}}) \cdot S_{\lambda,i} \cdot e^{-\sum_{j=1}^{i-1} \tau_{\lambda,j}} \quad (7)$$

where the subscripts i and j stand for the ith and jth layer, respectively.

An unusually broadened He I 10 830 Å profile is shown in Fig. 3a (dotted line). The two dips in the red wing are recognized to be due to the two telluric absorption lines at 10 832.11 Å and 10 833.98 Å. The dip near the top was caused by Sun-originated absorption by cloud-like material in front of the observed flare, which was also observed in this flare at other times. We will discuss this elsewhere. The computed profile is also plotted in Fig. 3a (solid line). The observed profile is well reproduced by dividing the flaring atmosphere along the line-of-sight into 30 layers, and each layer was taken as uniform and no limitation is applied to its thickness. The electron temperature T_e and (micro-turbulent) velocity ξ_t along the line-of-sight were taken to be 10^4 K and 8 km s^{-1} respectively for this profile. The corresponding distributions of τ_{03}, S and v_d are presented in Figs. 3b-d respectively. The macro-shift velocity v_{mac} is derived from the simulation to be 18 km s^{-1}.

Another two examples, observed in the impulsive and decaying phase, are shown in Figs. 4a and 4b (dotted line) respectively. The profile in Fig. 4a is narrower than that in Fig. 3a but still rather wide, and its non-Gaussian wings are not as apparent as that in Fig. 3a. I_{12} and I_3 are not separated. Once again we see the two dips on the red wings due to the two telluric lines. The observed profile is well generated by the above method. The computed profile is also presented in Fig. 4a (solid lines). The corresponding parameters have similar distributions to those in Figs. 3b-d. The fitting gives a macro-shift velocity of 40 km s^{-1} for this profile.

The profile in Fig. 4b has equivalent width and similar shape to that in Fig. 4a except that there is a moderate dip on the top. Components I_{12} and I_3 are separated and there is a swell on the blue wing. The calculated profile by the above method is plotted in Fig. 4b, too (solid line). The velocity of macro motion is 18 km s^{-1}. The distributions of corresponding optical depth, source function and Doppler velocity are similar to that above. However, there is a discontinuity on the curve of the distribution of Doppler velocity. Due to the discontinuous velocity distribution, the whole flaring plasma works as two separate plasma clouds, which have different macro-turbulent velocity and consequently resulted in the dip on the top of the profile.

The above simulations together with calculations of other profiles show that the expanding velocity decreases with time in a dynamical process. For example, for the temporal series of He I 10 830 Å profiles taken during the period from 01:10:54 UT to 01:19:31 UT that corresponds to a peak of 10 cm radio flux, the calculated expanding velocity decreases from greater than 120 km s^{-1} to about 20 km s^{-1}. The simulated expanding velocity in the impulsive phase is greater than that in the decaying phase, and the expanding velocity in the central part of the flare is lower than that in outer part of the flaring atmosphere. The source function and optical depth have similar distributions in the impulsive phase and decaying phase. However, the source function in the impulsive phase is greater than that in the decaying phase for a relative fixed position in the flaring atmosphere.

4. Discussion and conclusions

We studied the He I 10 830 Å profiles taken on 16 August 1989 during the 2N/X20 limb flare. Most of the observed profiles have an *FWHM* greater than 10 Å. We attempted to fit these profiles by Doppler broadening with a uniform flaring atmosphere model in two ways: large and small Doppler width. However, neither can fit the observed profiles well. On the contrary, He I 10 830 Å profiles of a rising post-flare loop and a flare-associated surge are Gaussian and can be well reproduced by simple Doppler broadening with a uniform model (Fig. 1b). These, together with the mentioned above, confirm that during the impulsive phase (and even in the main phase, as demonstrated above), He I 10 830 Å spectra of a flare are quite different in character from those of surges, jets or weak post-flare loops and cannot be simulated in the same way.

We investigated the impact of the Stark broadening on the He I 10 830 Å line profile by calculating the theoretical profiles using Doppler and Stark broadening mechanisms. The results indicate that in the flare atmosphere with generally accepted electron density, Stark broadening will not result in a discernible difference in the He I 10 830 Å line profile to that by Doppler broadening. In order for Stark broadening to produce an obvious effect on the He I 10 830 Å profile, the electron density should be greater than 10^{16} cm^{-3}, which is quite unrealistic. Is this flare really a special one which has such high electron density? We are inclined to think not, even though this needs to be confirmed by future observations and studies.

Recently, Fang et al. (2000) suggested that the broad profiles typically observed in solar limb flares are due to the effect of electron beams on the line source function. We (Ding & Li) have computed the influence of non-thermal electron beams on He I 10 830 Å line. The results show that electron beams will increase the line intensity obviously at low temperature (say below 10 000 K) and at high density and slightly broaden the line profile; we will discuss this in another paper. The impact of electron beams on

the He I 10 830 Å line is much less pronounced than on the Hα line because the He I 10 830 Å line is formed at higher temperature in the chromosphere where non-thermal effects are less significant (Fang et al. 2000). The slightly broadened line width and increased intensity cannot explain the extremely broadened He I 10 830 Å profiles.

Alternatively, we suggested an expanding flare model to interpret the observed He I 10 830 Å profiles. Generally, flaring plasma cannot move across the magnetic field lines in certain cases due to the constraint of magnetic flux tubes. Nevertheless, expansion could happen when field line is opened after the flare onset. Moreover, the pressure excess produced by rapid heating of the upper chromosphere is isotropic. The vertical component drives redshifts and blueshifts within the flux tube. If the magnetic field confining the chromospheric gas is sufficiently strong, it will prevent significant expansion of the flux tube. On the contrary, if the magnetic field is sufficiently weak, the adjacent flux tubes will be squeezed (Canfield et al. 1990). Expansion, in other words, will occur and the non-thermal electrons can still move along the magnetic field lines. Our observations resemble the latter case.

In our practical computation, we divided the flaring atmosphere into a certain number of layers and assume certain distributions of optical depth of the I_3 component, source function and Doppler velocity along the line-of-sight. Comparisons show that the suggested distributions of source function and optical thickness are consistent with the results of non-LTE computations we have made. Each layer was treated as uniform and contributes to the profiles by Doppler broadening. When an appropriate set of distributions of the above parameters is provided, this method can simulate the observed profiles very well, as demonstrated in Sect. 3.3. The distributions show that the atmosphere in the central part of the flare has larger optical depth and source function, and lower expanding velocity. We also tried to fit the observed profiles using other distributions, such as high expanding velocity and/or small source function. However, we cannot reproduce the observed profiles well by such distributions.

The expanding flaring atmosphere model is a possible explanation of the observed profiles. Even though the simulation from only one spectral line is not unique, the tendency of the distributions of physical parameters is reasonable. It indicates that the rapid heating of the chromosphere leads not only to downward chromospheric condensation and upward evaporation (Feldman 1990; Ding et al. 1996) but also to lateral expansion. The expanding velocity decreases with time in a dynamical process. The expansion was observed not only by our slit-jaw Hα photography (You et al. 1998) but by other authors (Gaizauskas 1986; Graeter & Kucera 1992) as well. This model must be confirmed by simultaneous observations and study in multiple spectral lines in the future.

He I 10 830 Å profiles of this flare show blue-shift velocity almost all of the time and the above calculations give blue-shift velocities of 2 to 40 km s^{-1} for the studied profiles. Our fitting process and results encourage us to conclude that there exists not only blue-shift velocity in this flare but an expanding velocity as well. The derived expanding velocities are generally several tens of km s^{-1}, and that for the widest profile is greater than 120 km s^{-1}. It can be a rapid lateral expansion along with a downward chromospheric condensation caused by non-thermal electron heating (You et al. 1998).

Acknowledgements. We thank the referee, Dr. P. Heinzel, for his valuable comments on this paper, and Dr. M. D. Ding for useful discussion. This work was supported by the National Natural Science Foundation of China (NSFC, grant number 49990451), National Basic Research Priorities Project (G2000078402) of China, and Chinese Academy of Sciences.

References

Canfield, R. C., Kiplinger, A. L., Penn, M. J., & Wülser, J.-P. 1990, ApJ, 363, 318

Ding, M. D., Watanabe, T., Shibata, K., et al. 1996, ApJ, 458, 391

Fang, C., Hénoux, J. -C., & Ding, M. D. 2000, A&A, 360, 702

Feldman, U. 1990, ApJ, 364, 322

Fisher, R. G., Canfield, R. C., & McClymont, A. N. 1985, ApJ, 289, 934

Gaizauskas, V. 1986, Morphology of Flaring Kernels with Asymmetrically-Broadened Hα Emission, in The lower atmosphere of solar flares, ed. D. F. Neidig, Sunspot, NSO/Sac Peak, 37

Graeter, M., & Kucera, T. A. 1992, Solar Phys., 141, 91

Ichimoto, K., Fang, G., & Hiei, E. 1993, He I 10 830 Å Observations at the Norikura Solar Observatory, in Proceedings of the first China-Japan seminar on solar physics, ed. G. X. Ai, et al. (Kunming Tondar Institute, Kunming), 158

Li, H., Fan, Z. Y., & You J. Q. 1999, Solar Phys., 185, 69

Lites, B. W., Neidig, D. F., & Bueno, J. T. 1986, The Visible Helium Spectrum of a White-Light Flare, in The lower atmosphere of solar flares, ed. F. F. Neidig, Sunspot, NSO/Sac Peak, 101

Wang, C. J., Lu, J., & You, J. Q. 1989, Acta Astron. Sin., 30, 87

Wang, C. J., Lu, J., Ni, Z. R., You, J. Q., & Fan, Z. Y. 1987, Acta Astron. Sin., 28, 101

You, J. Q., Wang, C. J., & Lu, J. 1989, Acta Astron. Sin., 30, 249

You, J. Q., & Oertel, G. K. 1992, ApJ, 389, L33

You, J. Q., Wang, C. J., Lu, J., & Fan, Z. Y. 1993, He I 10 830 Spectra of Small Flares, in Proceedings of the first China-Japan seminar on solar physics, ed. G. X. Ai, et al. (Kunming Tondar Institute, Kunming), 148

You, J. Q., Wang, C. J., Fan, Z. Y., & Li, H. 1998, Solar Phys., 182, 431